In-flight Performance of the Chandra High Resolution Camera

Stephen S. Murray, Gerald Austin, Jon Chappell, Joaquim Gomes
Almus Kenter, Ralph Kraft, Gary Meehan, Martin Zombeck*,
George Fraser†, Salvatore Serio‡

March 25, 2000

Abstract

The High Resolution Camera (HRC) is one of the two focal plane instruments on NASA's Chandra X-ray Observatory which was successfully launched July 23, 1999. The Chandra Observatory will perform high resolution spectroscopy and imaging in the X-ray band of 0.1 to 10 keV. The HRC instrument consists of two detectors, the HRC-I for imaging and the HRC-S for spectroscopy. In this paper we present an overview of the in-flight performance of the High Resolution Camera and discuss some of the initial scientific results.

1 Introduction

1.1 Launch

On July 23, 1999 at approximately 00:31 EDT, the Space Shuttle Discovery blasted off from the Kennedy Space Center carrying the Chandra X-ray Observatory (CXO) into orbit (Weisskopf et al.[1]. Included in this payload was the High Resolution Camera (HRC), one of the two focal plane instruments that are used to carry out scientific X-ray studies of the Universe. Using the Inertial Upper Stage solid rocket booster engine, and a series of firings of the Internal Propulsion System of the CXO spacecraft, Chandra was placed into a 10,000 km x 140,000 km elliptical orbit with about a 62 hour period. Transfer from the circular Shuttle orbit at 300 km to the final orbit took about two weeks during which the Observatory was allowed to outgas, and various spacecraft subsystems were turned on and checked out. The final CXO orbit takes the observatory through the Earth's radiation zones during which time the instruments are not operated. These radiation passes last about 12 hours leaving about 50 hours per orbit for scientific observing.

1.2 On-Orbit Activation and Calibration Phase

The On-orbit Activation and Calibration (OAC) program began with a period of intensive instrument checkout and calibration that spanned approximately 6 weeks. Numerous targets were

*Harvard-Smithsonian Center for Astrophysics, 60 Garden Street Cambridge, MA 02138
†University of Leicester, LE1 7RH, England
‡Osservatorio Astronomico G.S. Vaiana, I-90134 Palermo, Italy

In *X-Ray Optics, Instruments, and Missions III*, Joachim E. Trümper, Bernd Aschenbach, Editors,
Proceedings of SPIE Vol. 4012 (2000) • 0277-786X/00/$15.00

observed in order to establish such operating parameters as the proper focus of the telescope, the alignment of the optical axis, and the location of the instruments relative to the star camera. In addition, various known x-ray sources were observed for calibration purposes including standard candles for flux determination and pulsars for timing accuracy. All observations made during the OAC phase are in the public domain and can be accessed via the CXO archive. Some of these data are presented in this review.

The scientific program began on schedule, approximately 2 months after launch and consisted of a preplanned series of observations that had been selected by the various guaranteed time observers (GTO's); namely the instrument principal investigator teams, the telescope scientist, and the interdisciplinary scientists who made up the AXAF Science Working Group during the development of the observatory. After two months of GTO and continued OAC observations, the observatory operation expanded to include the full AO-1 guest observer (GO) program of targets. Approximately 70% of the total observing time consists of these GO targets. In the first six months of operation, Chandra has looked at over 500 targets and has achieved an operating efficiency in excess of 60%.

2 HRC Performance

2.1 Overview

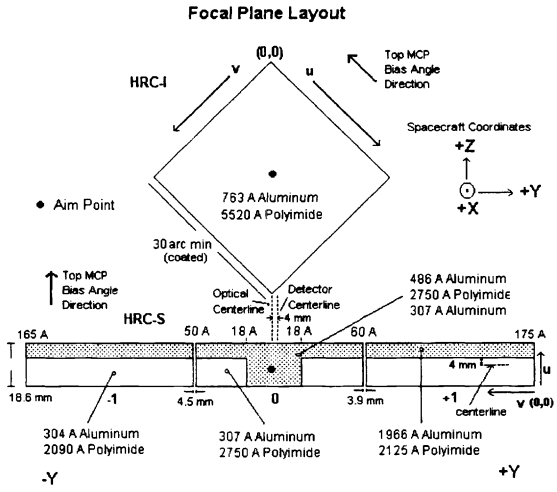

Figure 1: Schematic Diagram of the HRC Focal Plane

The HRC consists of two independent detectors designated HRC-I (imaging) and HRC-S (spectroscopy). The focal plane layout is shown in Figure 1. The HRC-I is a single $100 \times 100\,mm$ MCP and readout which is optimized for large field of view imaging (31 arc minutes), and an on-axis resolution of better than 0.5 arc seconds (FWHM). The X-ray telescope properties dominate the angular resolution off-axis. At 10 arc minutes off-axis, the angular resolution is about 10 arc seconds. More details on the HRC-I properties are given in this session by Kenter et al.[2]

The HRC-S is a set of three $100 \times 27\,mm$ MCPs arranged in a strip for a total of $\sim 300 \times 20\,mm$ active area. This detector is optimized as the readout for an objective grating spectrometer (LETGS Brinkman et al.[3]) that can be placed between the telescope and the detector for high resolution

spectroscopy. In particular, the outer two segments are tilted with respect to the center segment to approximate the curved surface of the spectrometer best focus (Rowland circle). Further details on the HRC-S are presented in this session by Kraft et al.[4].

The primary science objectives of Chandra are to study in detail X-ray sources, and to extend the sensitivity of previous X-ray missions by a factor of 10 or more in limiting flux. These goals require detectors that can sense individual X-rays with high efficiency, and with very low internal background. The HRC is designed to be a "faint object camera", limited to observing point-like sources with a count rate below $\sim 10\,ct\,s^{-1}$, and extended sources with a count rate below $\sim 150\,ct\,s^{-1}$. The telemetry limitation on Chandra permits a maximum of $184\,events\,s^{-1}$ to be recorded for transmission to the ground. Thus, a great deal of effort went into minimizing the internal background of the detectors through a careful choice of materials, and using special MCPs manufactured with low radioisotope glasses (cf. Chappell et al.[5], Garcia et al.[6], Fraser et al.[7]). However, it was also recognized that the on-orbit radiation environment could produce a substantial background contribution, particularly from cosmic rays. Thus, an active charged particle shield was included in the design.

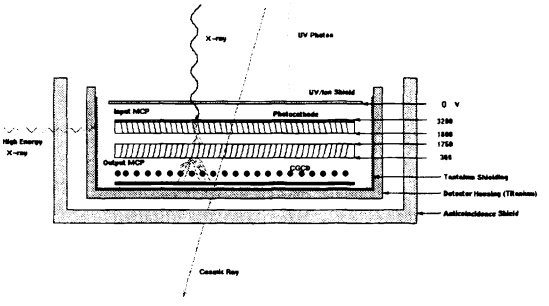

Figure 2: Cartoon representation of the HRC Detector. Illustrates the main components: UVIS; CsI coated chevron pair of MCPs; CGCD; radiation shielding; vacuum housing; and active coincidence shield.

Each of the detectors consist of an Aluminized polyimide UV/Ion Shield (UVIS), a CsI coated MCP chevron pair, and a Crossed Grid Charge Detector (CGCD) readout. They are housed in a vacuum enclosure. Surrounding the housing is a five sided plastic scintillator shield which is viewed by a photomultiplier tube (PMT) to provide anticoincidence signals for background reduction. A schematic representation of the detector is shown below in Figure 2.

2.2 Performance

2.2.1 Background

The initial turn on of the HRC was delayed for about a week when it was found that the detector counting rate while out of the telescope focus was much higher than expected. In retrospect, it was determined that this high background rate is due to charged particles (cosmic rays) that are incident on the detector in the High Earth Orbit where the Earth's magnetic field no longer acts as a shield. Solar particles and galactic cosmic rays produce an isotropic flux of about $2\,ct\,cm^{-2}s^{-1}$ at the Chandra orbit. The CsI coated MCP of the HRC has almost 100% detection efficiency for these particles. The resulting high count rate $(200 - 250\,ct\,s^{-1})$ exceeds the telemetry event limit

on Chandra ($184\,events\,s^{-1}$) and would introduce serious dead time problems if it were not possible to identify these events on-orbit and suppress them from the data stream.

To reduce the background from charged particles an active plastic scintillator coincidence shield surrounds the MCPs. Detector events in coincidence with a shield signal are vetoed by the on board processing electronics and do not enter the data stream. For the HRC-I, the shield is very efficient and detects over 99.5% of minimum ionizing cosmic rays. However, some of the charged particles are of solar origin and have low enough energy ($\sim 100 - 200\,keV$) that they are stopped in the MCPs and do not produce a veto signal in the shield. These events are not distinguishable from valid X-ray induced events and are therefore contributors to the overall instrument background. The typical quiescent rate observed in the HRC-I (imaging detector) is about ($40 - 50\,ct\,s^{-1}$) over the full active area ($100\,cm^2$) of the detector. During ground testing, the background rate was typically only $10\,ct\,s^{-1}$.

In the case of the HRC-S, there is a timing error in the MCP trigger relative to the shield events and very few veto signals are generated. Thus the background in this detector is high. To overcome the high counting rate and subsequent telemetry saturation, the HRC-S operation has been modified using the edge blanking feature of the processing electronics. Since the HRC-S is used to read out the dispersed spectrum of an X-ray source (created by the grating spectrometer, see Brinkman et al.[3]), only a small region of the detector is actually needed - i.e., a long strip of the detector only a few millimeters wide. Edge blanking allows the electronics to accept events only within a rectangular region of interest, thus limiting the total active area of the detector and reducing the event rate to a level well below telemetry saturation. For normal spectroscopic observations, the HRC-S active region is reduced to a $300 \times 9.6\,mm$ strip, resulting in a quiescent background rate of $< 100\,ct\,s^{-1}$.

The root cause of the timing error in the veto signal has been examined using the engineering model of HRC. The HRC uses a trigger signal taken from the output of the MCP to initiate event timing. Different MCPs are used for HRC-I (Galileo Electro Optics Corporation (GEOC); now Burle) and HRC-S (Philips Photonics; now Photonis SAS) and these devices have different chemical and electrical characteristics. Because of their lower plate resistance, the rise time of the MCP trigger signal for HRC-S is significantly faster than for HRC-I and the time window for accepting a veto from the shield occurs too soon for HRC-S. The timing error is estimated to be about $1\,\mu sec$, and there is no adjustment available from the ground to alter this parameter.

2.2.2 Efficiency

The detection efficiency (HRC-I and HRC-S) is close the expected levels derived from the pre-launch calibration. Details are given by Kenter et al.[2] for HRC-I and Kraft et al.[4] for HRC-S. Overall, the detectors have a peak response (including the telescope and filters) at about $1\,keV$ with an effective area of $\sim 250\,cm^2$, as shown in Figures 3 and 4.

2.2.3 Image Quality

The HRC has an intrinsic spatial resolution of $\sim 20\,\mu m$ FWHM, determined during the subassembly calibration of both flight units. The Chandra X-ray telescope has a HPD of about $1\,arcsec$ which translates to $\sim 50\,\mu m$ in the focal plane, and the residual errors from the aspect reconstruction of an image are typically $< 0.1 - 0.3\,arcsec$. During the OAC phase a number of focus plates were

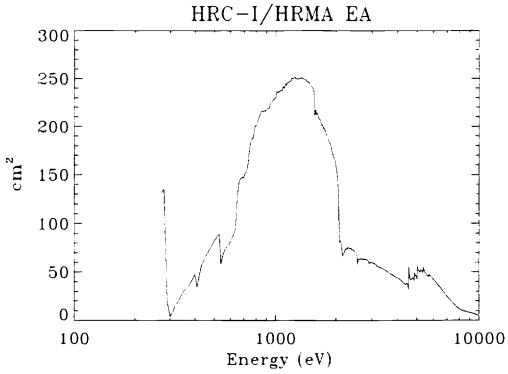

Figure 3: HRC-I effective area vs. energy for an on-axis source.

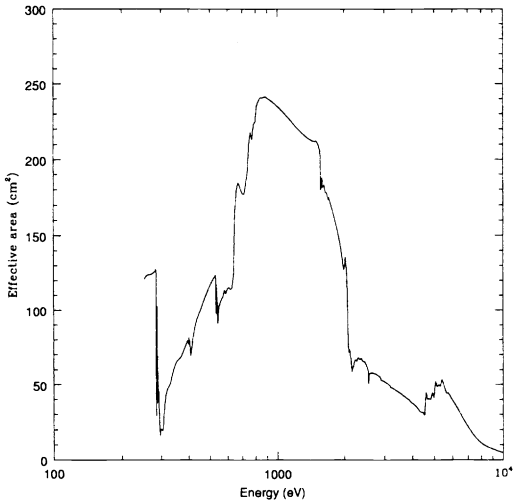

Figure 4: HRC-S effective area vs. energy for an on-axis source.

obtained using a point source on-axis (typically these were 1000 sec observations of the stellar source ArLac giving 2000-3000 counts in the image). At the best focus the encircled energy plot agrees very well with the pre-launch. The HRC-I measured PSF has 50% of the source counts within a $0.75\,arcsec$ diameter, and 90% within $1.8\,arcsec$ diameter. This is shown in Figure 5. A similar result was obtained for HRC-S.

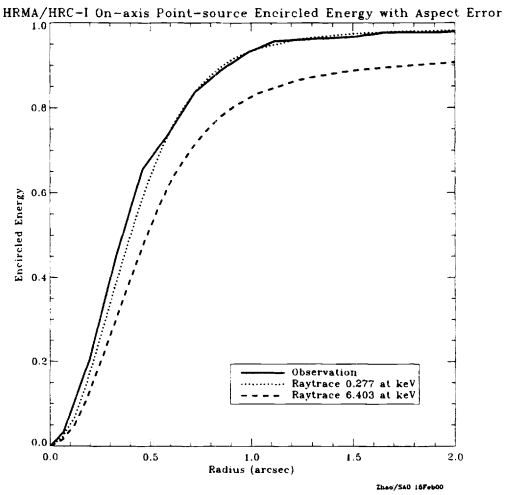

Figure 5: Observed encircled energy versus radius compared with telescope predictions including aspect blur and HRC resolution.

Imaging Problems: Despite the close agreement of the PSF with pre-flight predictions, close inspection of the HRC-I images of bright point sources have uncovered several irregularities. First, there is a "ghost" image associated with bright sources where a few percent of the flux is mislocated by about $0.5\,mm$ and spread out in the general direction of the detector U-axis. This behavior was noted during the ground calibration and is due to events where the pulse amplitude causes saturation in the readout amplifiers or the charge cloud from the MCPs is unusually broad. In either case it is possible to screen against these events and reduce the mislocated events from a few percent to less than a tenth percent of the source flux Murray et al.[8].

A second source of image blur is electronic ringing that is sometimes introduced at the analog to digital signal processing stage when the estimated coarse position is switched by one location. This effect happens only when events have large amplitude and are initially located in the negative half of a readout tap (a more detailed description of the problem is given by Murray et al.[8]). The effect on an image is to add a blur of about 0.1-0.3 arc seconds. During the OAC phase, it was found that the high voltage setting for HRC-I had been initially set too high resulting in a high fraction (>50%) of events susceptible to the image blur effect. Also, the set point of the range switch threshold (a gain adjustment for the processing electronics) had been set too low. Changes to both of these parameters (lower high voltage and higher range switch threshold) result in less than 30% of events (on axis where the MCP gain is highest) being susceptible to image blur. An added benefit of these operating changes is a lower fraction of "ghost" events. An investigation is in progress to correct the error introduced by ringing (Murray et al. [8], and Juda et al.[9]) which will be reported at the next annual SPIE meeting (45-th Conference, July 2000).

A third area of image degradation is the discovery of image blur that is correlated with the dither motion of the observatory. In order to avoid high local count rates on individual MCP pores,

and to spread the charge extraction over as many pores as possible to extend the MCP lifetime, the observatory executes a two dimensional small amplitude motion while observing. This dither pattern is a Lissajous figure with amplitude of 20 arc seconds (40 arc seconds peak-to-peak) and periods of about 1087 and 769 seconds in each direction (spacecraft y and z which are at about 45 degrees to the detector readout axes). A result of this motion is that the HRC de-gap map is sampled over at least one gap in each axis, and possibly two gaps. If there are any residual errors in the de-gap maps, these will manifest as a blur in the de-gapped and aspect corrected image. There are preliminary indications of 2-4 HRC pixel effects for strong on-axis sources that are currently under investigation. The status of this investigation will be reported at this Conference and also at the annual SPIE summer 2000 meeting (Murray et al.[8]).

3 Science Observations

3.1 OAC Phase Observations

3.1.1 PSR0540-69

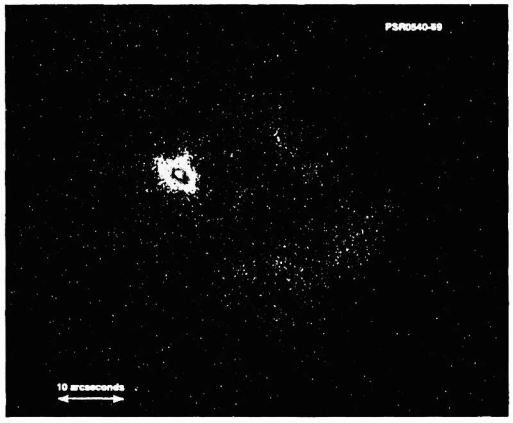

Figure 6: Pulsar PSR0540-69 HRC-I Image

One of the first science/calibration targets using the HRC was an observation of the pulsar PSR0540-69 (Kaarat et al.[10]). This is a Crab-like supernova remnant in the Large Magellanic Cloud that contains a known $50\,msec$ pulsar embedded in a synchrotron nebula. Figure 6 shows the HRC image of this source, which was taken in September 1999. The detector was slightly out of focus (by about $250\,\mu m$) since the analysis of focus data had not yet been completed. The bright central source is the X-ray pulsar which can be seen clearly against the more diffuse nebula, which is embedded in a faint expanding shell.

An FFT analysis of the photon arrival times for events within 1 arc second radius of the pulsar is shown in Figure 7. There is a clear signal at the expected pulse period. Closer examination of the event arrival times using a period folding analysis gives a pulse period (after barycentric corrections) of 0.0505081 sec and a light curve shown in Figure 7. The observation demonstrates the timing accuracy of the HRC as well as the outstanding image quality.

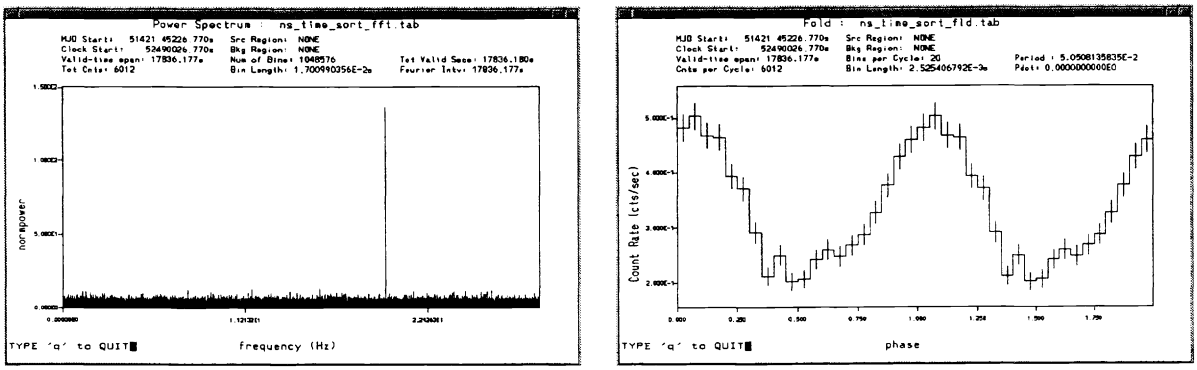

Figure 7: FFT and Light Curve for the Pulsar PSR0540-69

3.1.2 Cen-A

The nearest active galactic nucleus Cen-A was observed with the HRC-I as a calibration target to test the imaging capabilities of the detector. The target has a point-like bright central object corresponding to the supermassive black hole at the galaxy center, extended emission associated with the underlying galaxy, numerous point sources associated with x-ray binaries in the galaxy, an X-ray jet extending to the north-east from the nucleus, and diffuse x-ray emission associated with the radio lobes that characterize this FR-I radio galaxy. All of these features can be seen in the initial HRC-I image that has been analyzed by Kraft et al.[11], and is reproduced here in Figure 8.

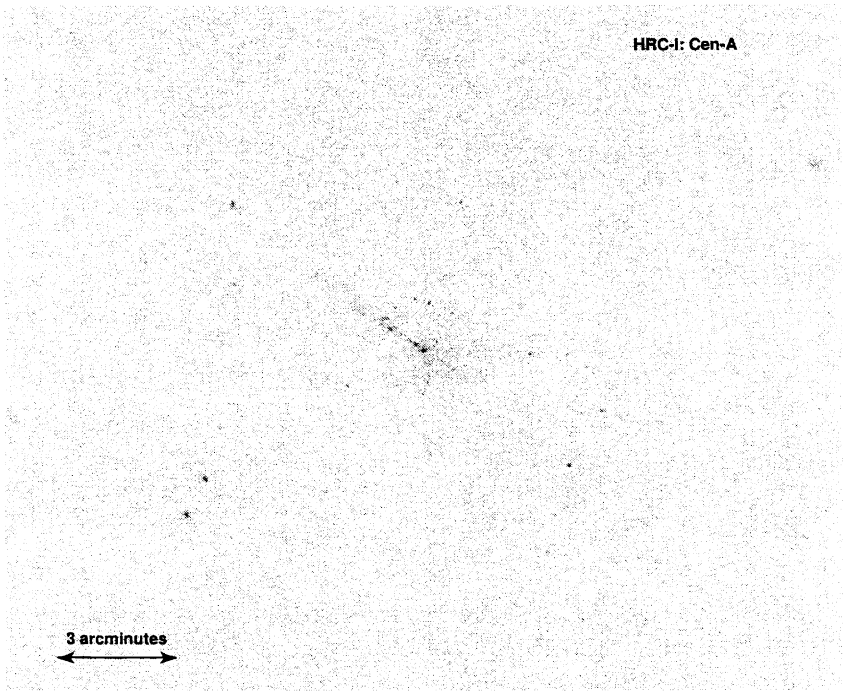

Figure 8: HRC-I observation of the nearby AGN and Radio Galaxy Cen-A

The observation was also taken while the HRC-I was slightly out of focus. This observation was

made with the HRC pre-launch high voltage and range switch settings which contribute to a high fraction of mislocated events. Despite these image imperfections Kraft et al. were able to measure an upper limit to the extent of the nuclear source of a few tenths of an arc second. A detailed comparison of the X-ray and radio features of Cen-A place constraints on the mechanisms and physical conditions that are producing the radiation.

3.1.3 Cas-A

The official first light image from Chandra was of the young supernova remnant Cas-A. That image was obtained using the Advanced CCD Imaging Spectrometer and showed the existence of a point-like source near the center of the explosion. This source is believed to be associated with the expected compact object (either a neutron star or black hole) that is produced in the core-collapse supernova explosion. The outstanding angular resolution of the Chandra X-ray telescope made the detection of this source against the diffuse emission of the remnant possible. Shortly thereafter, the HRC-I and HRC-S were also used to image Cas-A. These were primarily meant as flux calibration observations; however, with the discovery of a possible compact object, the HRC timing capabilities were used to search for a possible period that would identify this object as a neutron star.

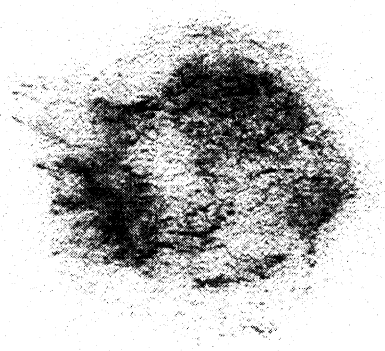

Figure 9:

Figure 9 shows the HRC-I image of Cas-A and clearly confirms the presence of a point source near the center. Careful studies show this source to be unresolved at the 0.5 second level. In this 10,000 second observation only 300 photons are detected from the central object. This is not enough data to carry out a detailed period search, particularly if the modulation fraction is not very high. Thus, there is as yet no direct timing information to confirm that the central object is a neutron star. A longer HRC-I observation of 50 ksec using proprietary GTO time has been carried out and it currently being analyzed.

3.2 Proprietary Observations

Some of the HRC Team GTO observations have been completed at the time of this paper and are summarized in the sections below. These are not yet fully analyzed as there are many detailed complications in the Chandra data from both the HRC and the ACIS that still being calibrated and understood. These summaries are meant to illustrate the range of capabilities of the Observatory and the scientific advances that Chandra makes possible. The final science analysis for these and other Chandra observations will be reported in the appropriate astronomy literature.

3.2.1 Andromeda - M31 Transient Monitor

The HRC monitoring program for M31 consists of monthly observations of the galaxy, in a mosaic of five HRC-I pointings to cover the central 2.5 degrees of the galaxy, to detect the onset of X-ray emission from transient or periodic sources. In addition, each month a single ACIS observation is made of any interesting source to obtain spectral information and to fill in the light curve from the HRC. In the first monthly scan, a transient source was detected about 30 arc seconds from the center of the galaxy (Garcia et al.[12]). The discovery image is shown in Figure 10 with the sources marked.

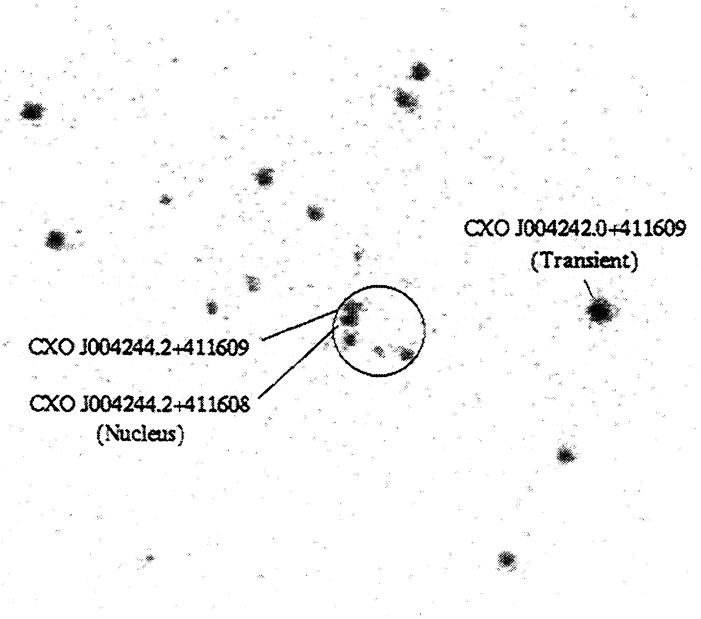

Figure 10: Central region of the galaxy M31 (Andromeda) showing the newly discovered transient source and the complex of sources at the nucleus.

Also seen in this image is the complex of X-ray sources located at the center of M31 where a supermassive back hole of $3 \times 10^7 M_\odot$ has been identified. There are five sources within 5 arc seconds of the nucleus, one appears to coincide with the back hole at the limit of location precision of the data - about 1 arc second. Both the transient and nuclear sources are interesting objects. The transient may well be an example of a stellar mass black hole detected outside of our galaxy which will improve our understanding of these unusual objects. The nuclear source appears to be less luminous than expected, and it has a surprisingly soft X-ray spectrum. Both of these properties are inconsistent with the standard models for X-ray emission from such a source.

3.2.2 M82 - A Starburst Galaxy

The relatively nearby irregular galaxy M82 is believed to have been disrupted by the near passage of another galaxy only a few hundred million years ago. A consequence of this interaction has been the triggering of rapid star formation in M82 (hence the designation Starburst galaxy). It is estimated that a supernova occurs in M82 every 10 years. The observations of M82 are designed to study the number of variable sources in this galaxy and their distribution in luminosity, variability amplitude and time scale, and their correspondence to radio and optical counterparts.

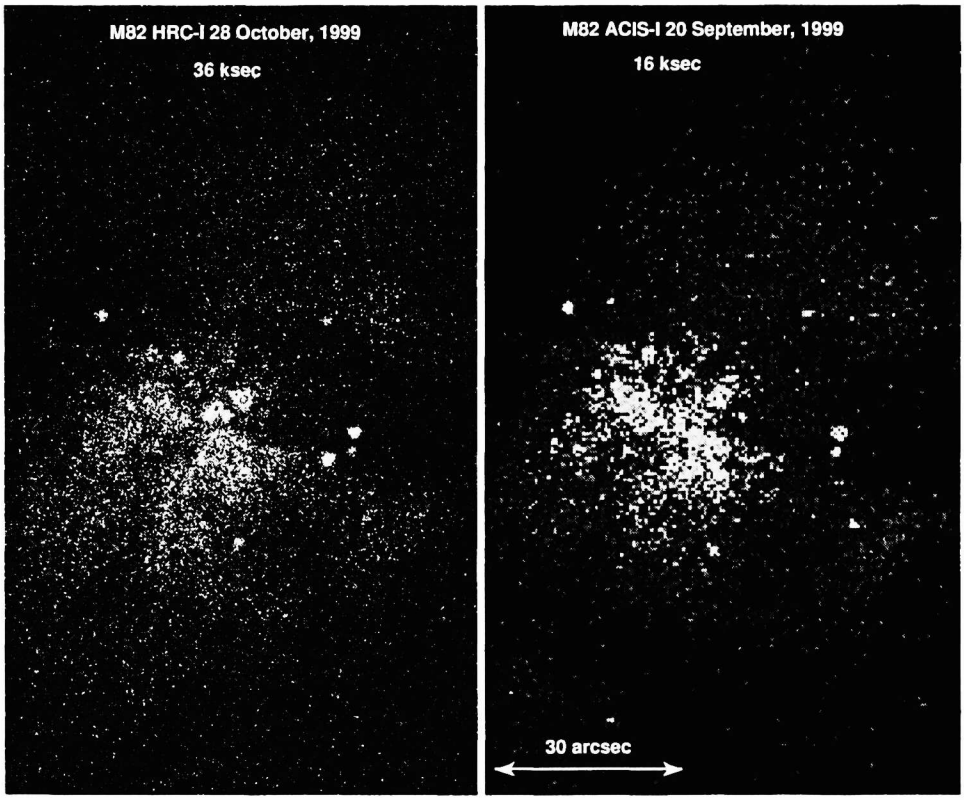

Figure 11: Galaxy M82. Two images taken about one month apart illustrates variability of some sources.

Figure 11 shows two images of M82 taken about one month apart. Visual inspection shows the presence of three highly variable sources, two that were "on" in the October 28, 1999 observation and one that was "on" in the earlier September 20, 1999 observation.

3.2.3 Lockman Hole - A Deep Survey

The Cosmic X-ray Background (CXRB) was first discovered in the early 1960's along with the detection of the first non-solar X-ray source (Giaconni et al.[13]). The origin of this background has been a topic of research ever since its discovery with more attributed to discrete sources as more sensitive observations are made. Prior to Chandra, the deepest image in X-rays was a 1.2 million second observation of a region in the Northern sky known as the Lockman Hole (so named for the very low hydrogen column density along the line of sight). The HRC-I was used to observe this same area for 300 ksec, of which the first 100 ksec have been processed and analyzed.

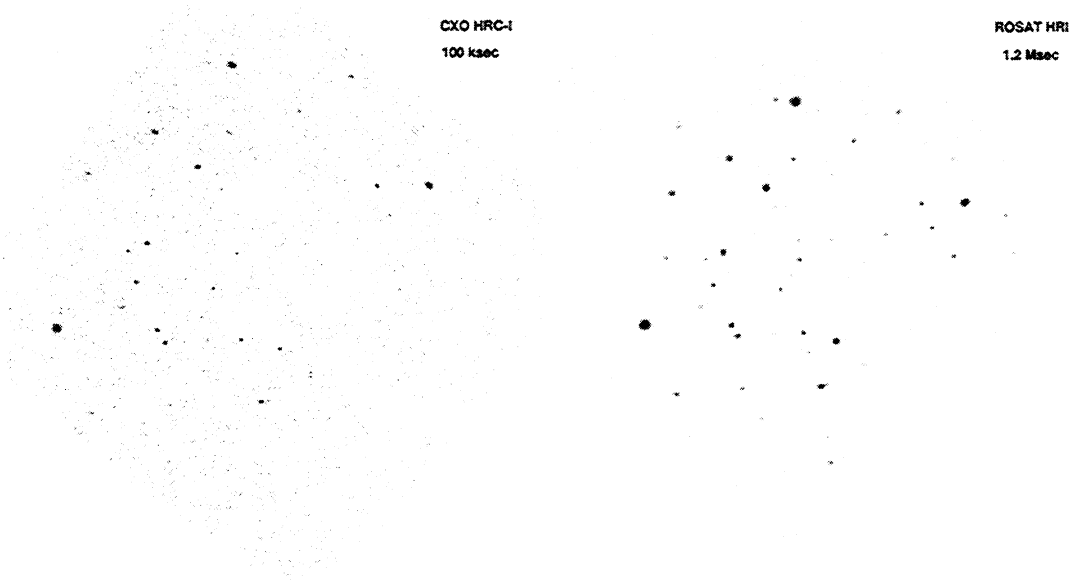

Figure 12: Chandra HRC-I and ROSAT HRI images of the Lockman Hole.

Figure 12 shows the HRC-I image after the first 100 ksec of the observation. It can be compared to the longer composite ROSAT image of the same region. All of the sources found in the ROSAT observation have been detected in the Chandra data. The limiting flux for the 100 ksec observation is about two times fainter than the ROSAT limit, a result of the higher angular resolution of Chandra.

4 Conclusions

The Chandra X-ray Observatory has been in operation for about 1/2 year and has already produced remarkable results. The X-ray telescope is outstanding, giving sub-arc second images over the entire 0.1 - 10 keV band. Both focal plane instruments are operating and returning excellent science data. The detectors have experienced some problems that have been dealt with through changes to operating conditions and improved ground based data processing. The objective grating spectrometers both work as expected yielding the highest resolution spectra ever obtained for non-solar celestial X-ray sources.

Chandra operations have gone very smoothly with only a few problems, all of which were traced to procedural errors rather than malfunctions of spacecraft systems. The spacecraft has met all of the performance requirements and appears to be stable and robust. The observatory lifetime is 5 years nominal, with >15 years as a goal.

References

[1] Weisskopf et al., "Chandra X-ray Observatory Overview", SPIE [*4012*], 2000.

[2] Kenter et al., "In-flight Performance and Calibration of the Chandra High Resolution Camera Imager (HRC-I)", SPIE [*4012*], 2000.

[3] Brinkman et al., "Description and Performance of the Low-Energy Transmission Grating Spectrometer on board Chandra", SPIE [*4012*], 2000.

[4] Kraft et al., "In-flight Performance and Calibration of the Chandra High \\ Resolution Camera Spectroscopic Readout (HRC-S)", SPIE {*4012*}, 2000.

[5] Chappell et al., "Background Reduction in Microchannel Plates", SPIE [*1344*], 1990.

[6] Garcia et al., "Low Noise Microchannel Plate Detectors for X-ray Astronomy", SPIE [*1140*], 1989.

[7] Fraser et al., "Developments in Microchannel Plate Detectors for X-ray Astronomy", SPIE [*597*], 1986.

[8] Murray et al., "Event Screening for the Chandra High Resolution Camera", SPIE [in preperation], 2000.

[9] Juda et al., "Improving Chandra HRC Event Positions via Corrections to Crossed-Grid Charge Detector Signals", SPIE [in preparation], 2000.

[10] Kaaret et al. "Chandra Observation of PSR0540-69", ApJ Letters [submitted], 2000.

[11] Kraft et al., "A Chandra High-Resolution X-ray Image of Centaurus A", ApJ Letters [*531L*], 1999.

[12] Garcia et al., "A First Look at the Nuclear Region of M31 with Chandra", ApJ Letters (submitted), 2000

[13] Giacconi et al., Phys Rev Letters [*9*], 1962